AIAA JOURNAL
Vol. 46, No. 1, January 2008

Near-Field Investigation of Chevron Nozzle Mechanisms

B. Callender* and E. Gutmark†
University of Cincinnati, Cincinnati, Ohio 45221
and
S. Martens‡
GE Global Research, Niskayuna, New York 12309

DOI: 10.2514/1.17720

A detailed investigation into the effect of chevron nozzles on the near-field acoustics of a separate flow exhaust system was conducted at the University of Cincinnati Anechoic Test Facility. Chevrons with varying numbers of lobes and levels of penetration were selected to provide insight into the effects of these geometric parameters on the acoustic near field. Tests were conducted at two different nozzle operating conditions and the chevrons were shown to produce substantial modifications to the near field over a wide range of frequencies. The chevrons were most effective at lower frequencies where the peak noise region was reduced by 5–7 dB and dramatically reduced in size. At higher frequencies, the chevrons provided strong noise suppression downstream of approximately seven equivalent nozzle diameters with increases closer to the nozzle lip. The nozzle penetration was shown to have the most significant impact on the acoustic near field with more subtle differences being seen with respect to the number of chevron lobes.

Nomenclature

f	=	frequency
M	=	jet exhaust Mach number
St	=	Strouhal number
T	=	temperature
V	=	jet exhaust velocity
V_{mix}	=	mixed velocity, mass averaged velocity
V_{shear}	=	nozzle shear velocity ($V_p - V_s$)

Subscripts

o	=	total or stagnation property
p	=	primary or core flow
s	=	secondary or fan flow

I. Introduction

CHEVRON nozzles represent the current state of the art in jet noise reduction technology for application in medium to high bypass ratio turbofan engines. These nozzles feature triangular serrations in the nozzle trailing edge, which induce streamwise vorticity into the shear layer. As with tabbed nozzles, this vorticity leads to increased mixing and reduced jet plume length [1–5]. As opposed to other noise reduction technologies, such as forced mixers, chevron nozzles are capable of reducing engine exhaust noise while imposing minimal engine performance penalty and a nearly insignificant weight impact [6–8]. An extensive effort conducted by researchers at NASA Glenn Research Center identified a set of chevron nozzle configurations providing reductions in the jet component of effective perceived noise level (EPNL) of 2–3 EPNdB with minimal loss of nozzle thrust [6]. However, at the present time, there have been few published works seeking to improve the understanding of the fundamental mechanisms responsible for the acoustic benefit of chevron nozzles. The results of a far-field acoustic investigation of chevron nozzle trends conducted at the University of Cincinnati were recently published by the current authors [9]. The results of this study showed that the nozzle operating condition, particularly the shear velocity between the core and fan streams, can strongly influence the effectiveness of a given chevron design. This study identified consistent trends attributable to the chevron geometry by considering two different levels of penetration as well as the number of chevrons. The penetration was concluded to have the largest impact on the acoustic benefit as it was seen to influence spectral sound pressure level (SPL) at all measured frequencies and angles. In contrast, the number of lobes was seen to primarily affect higher frequencies. Although this investigation provided a great deal of insight into the impact of various chevron parameters on the acoustic far field, it did not allow many definitive conclusions to be reached in regard to the physical mechanisms responsible for these changes. This investigation is a followup to this previous study and seeks to gain more understanding of the chevron effect on the acoustic sources and propagation.

II. Test Setup and Facility

Acoustic data were collected at the University of Cincinnati Anechoic Test Facility. This facility features a coaxial flow test rig capable of accurately simulating separate flow exhaust nozzle conditions in terms of nozzle pressure ratio and shear velocity ($V_p - V_s$). For the current series of tests, the rig is fitted with a scale model separate exhaust system with core and fan areas of 3.6 and 12.5 in.^{2}, respectively. A photograph of the baseline nozzle configuration is shown in Fig. 1. Complete details of the test rig and its capabilities are available in [10].

Four core nozzles were investigated in this study including a baseline conic nozzle and three different chevron nozzles. The chevron nozzles were selected to provide insight into the effect of the number of chevrons as well as the level of penetration of the chevrons into the flow. One nozzle was a 12 lobe design with a nominal level of penetration on the order of the boundary layer thickness. The other two nozzles each featured eight chevrons. One had the same nominal level of penetration as the 12 lobe nozzle and the other nozzle had approximately twice the level of penetration. Figure 2 shows a photograph of the four chevron nozzles used in the study, while the geometric details are summarized in Table 1. A conic fan nozzle was used for all tests.

Presented as Paper 3210 at the 9th AIAA/CEAS Aeroacoustics Conference, Hilton Head, SC, 12–14 May 2003; received 17 May 2005; revision received 16 February 2007; accepted for publication 27 February 2007.

*Currently Engineering Team Leader, Acoustics and Installation Aerodynamics, GE Aviation, Cincinnati, OH. Member AIAA.

†Ohio Eminent Scholar and Professor, Aerospace Engineering and Engineering Mechanics. Associate Fellow AIAA.

‡Mechanical Engineer, Energy and Propulsion Technologies. Senior Member AIAA.

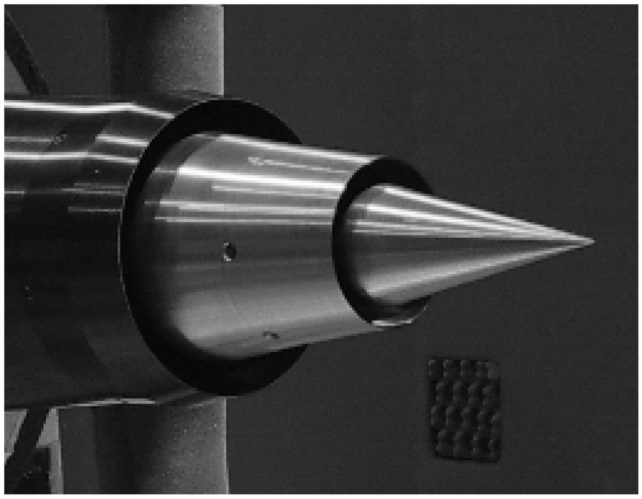

Fig. 1 Photograph of separate flow exhaust model.

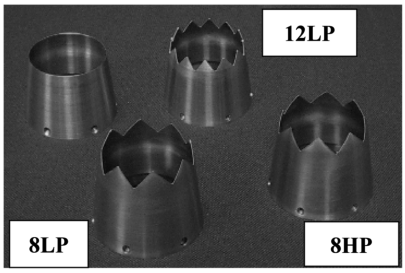

Fig. 2 Photograph of core nozzles used in the study.

Both far-field and near-field acoustic data will be presented in this work. All acoustic measurements were obtained using Bruel and Kjaer model 4939 1/4 in. condenser microphones. These microphones have an upper frequency range of 100 kHz and were powered by Nexis® model 2690-AS04 signal conditioning amplifiers. Acoustic data were acquired as a binary time series record using a pair of synchronized National Instruments model 4452 dynamic signal acquisition boards and postprocessed using custom developed LabView® codes.

Far-field measurements were acquired on a 12.5 ft radius microphone array. This array provided coverage of nozzle directivity angles from 70 to 150 deg, with the directivity angle being defined from the inlet direction. Near-field mappings were obtained using a Velmex 9000 three-axis traversing system. Using a rake of eight microphones, spaced 6.25 in. apart, this system was used to map a rectangular area consisting of approximately 10 equivalent nozzle diameters in the axial direction and six diameters in the radial direction. Figure 3 shows a schematic view of the University of Cincinnati (UC) acoustic test chamber, with the layout and location of the far-field array as well as the near-field mapping zone indicated. A photograph of the microphone rake attached to the traversing system is shown in Fig. 4. The microphone rake was designed to minimize any potential reflections by isolating the microphones forward of the rake's primary structure. Although the floor beneath the traversing system was acoustically treated, the system itself and its associated support structure was not. It was recognized that some

Table 1 Nozzle geometry summary

Nozzle	No. of chevrons	Penetration
Baseline	0	Baseline
12LP	12	Nominal
8LP	8	Nominal
8HP	8	Increased

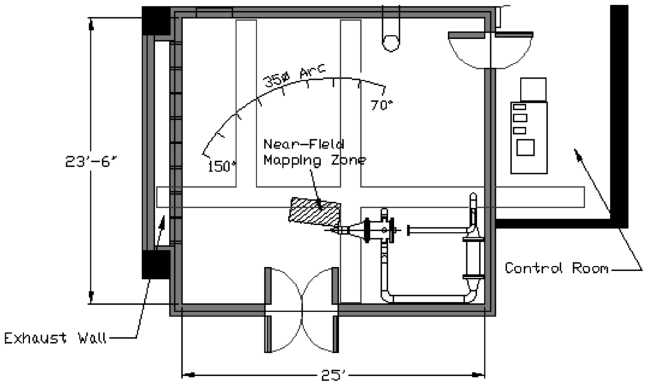

Fig. 3 Layout and dimensions of UC acoustic test facility.

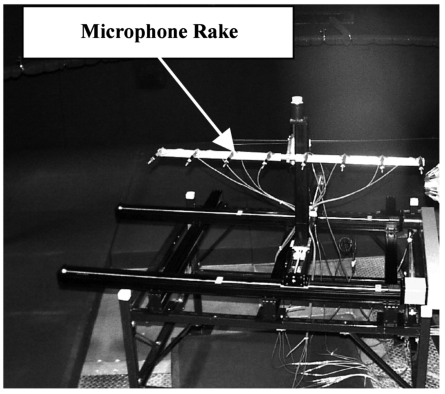

Fig. 4 Photograph of microphone rake used for near-field mapping study.

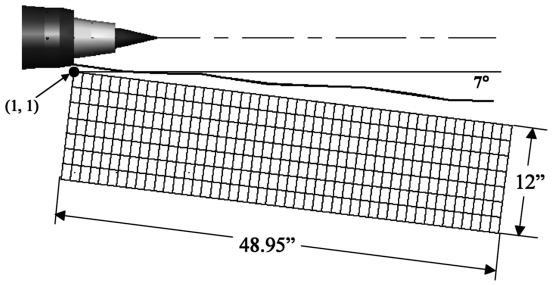

Fig. 5 Grid setup and orientation used to collect near-field data; 384 point grid; axial resolution: 1.04 in., radial resolution: 1.71 in.

level of reflection would be present as a result of this. However, it was not the intention of this study to accurately determine absolute near-field noise levels, but rather capture qualitative changes, such as changes in directivity patterns and noise levels relative to the baseline. Therefore, a fully anechoic environment was not deemed necessary for this study. The positioning of the traverse system and microphone acquisition was controlled by a custom written LabView code. This control code allowed the mapping grid to be matched to the jet divergence angle to avoid any direct flow impingement on the microphones.

The grid geometry and orientation used in this study is shown in Fig. 5 and was sized to balance the grid size and resolution with the time required to complete the grid mapping. The 384 point grid covers 48.9 in. in the axial direction and 12 in. in the radial direction resulting in axial and radial resolutions of 1.04 and 1.71 in., respectively. The grid was oriented on a 7 deg divergence angle with the origin positioned 3/4 in. from the fan nozzle lip. The 7 deg divergence angle was fixed for each of the four test nozzles so that the grid points would remain constant for the various nozzle mappings. As it is known that mixing devices such as chevrons impact the

spreading rate of the jet, consideration was given to matching the grid divergence angle to that produced by each particular nozzle. However, this would have resulted in each mapping being in a slightly different location relative to the jet centerline. For this reason, it was decided to maintain the grid on a fixed divergence angle to allow more accurate comparison of the mappings. The value of 7 deg was selected based on a measure of the spread of nozzle 8HP.

The measurement uncertainty of the data acquisition system for far-field acoustic acquisitions has been established to be within ± 0.2 dB for back-to-back acquisitions [11]. This is based on a control system accuracy that maintains the standard deviation of the core and fan velocity at less than $\pm 1\%$ of the set point value. All of the data presented in this work were acquired within this level of control accuracy. To establish the expected variation in the near-field measurements, a comparison was made between two baseline repeats. Comparison of these measurements established that the data presented in this work repeats within a standard deviation of ± 0.7 dB at any grid position and frequency band.

III. Results and Discussion

Data for two different operating conditions will be presented in this work. For both operating conditions, the core flow was maintained at a nozzle pressure ratio (NPR) of 1.85 and a total temperature (T_o) of 250°F. This corresponds to a core flow Reynolds number on the order of 9.5×10^5. The fan flow was maintained at a T_o of approximately 60°F with the pressure ratio being adjusted to set the desired exhaust system shear velocity. Table 2 defines the two operating conditions that were tested and indicates the shear velocity as normalized by the mass averaged velocity of the core and fan streams, denoted by V_{mix}. The fan Reynolds number varied from 7.8×10^5 at the high shear condition to 1.6×10^6 at the nominal shear condition. For all test conditions, both the core and fan stream Reynolds numbers were maintained above the 4.0×10^5 level recommended by Viswanathan [12] to avoid noise contamination due to scaling effects.

Far-field results from the previous study by the current authors showed that the chevrons were most effective at lower frequencies with reduced effectiveness observed at the higher frequencies. At the high shear operating condition, far-field spectra showed a strong spectral crossover at higher frequencies. To lend more understanding to this spectral variation, SPL mappings will be presented for two different frequencies. Far-field one-third octave spectra at the peak emission angle of 150 deg are shown for the high shear condition in Fig. 6. Note that the frequency is normalized as a Strouhal number using the equivalent nozzle diameter and the mixed jet velocity, V_{mix}. From these results the spectral variation in the chevron acoustic benefit is quite clear. Two different Strouhal numbers were selected for analysis in this work. The first represents the point of maximum low-frequency chevron noise reduction, which corresponds roughly to the peak jet noise frequency. Additionally, the Strouhal number corresponding to the point of maximum high-frequency crossover was also selected. Figure 7 shows the acoustic spectra at the peak jet noise emission angle for the nominal shear condition. Although there was no crossover at this condition, the high frequencies do show a reduced SPL benefit relative to the mid and low frequencies. The Strouhal numbers selected for analysis at this operating condition correspond to the same model scale frequencies as selected for the high shear operating condition. Therefore, the value of the selected Strouhal numbers will be slightly different for each condition. The selected Strouhal numbers for each operating condition are noted in Figs. 6 and 7. Figures 8–13 show far-field overall sound pressure level (OASPL) directivity as well as the directivity of selected Stouhal numbers. These plots will be referenced throughout to illustrate the consistency seen between the far- and near-field results. All near-field mappings correspond to an azimuthal plane which intersects the chevron peak.

Table 2 Summary of test conditions

Operating point	Core NPR	$To,_p\,(R)$	$To,_s\,(R)$	$V_{\text{shear}}/V_{\text{mix}}$
Nominal shear	1.85	710	520	0.58
High shear	1.85	710	520	1.12

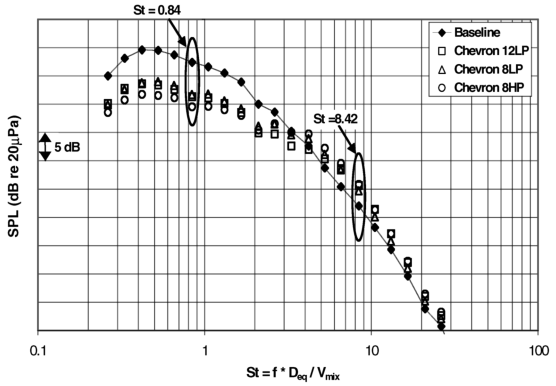

Fig. 6 High shear condition far-field spectra; directivity angle: 150 deg; mixed velocity Strouhal numbers selected for mappings are noted.

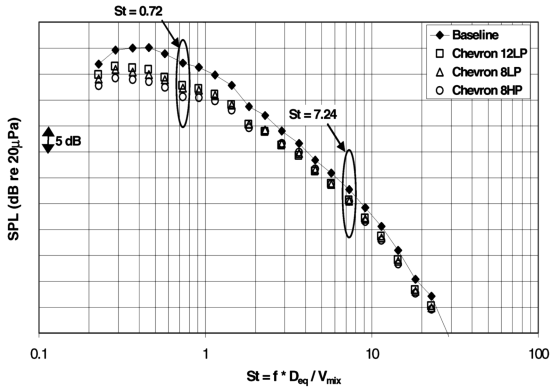

Fig. 7 Nominal shear condition far-field spectra; directivity angle: 150 deg; mixed velocity Strouhal numbers selected for mappings are noted.

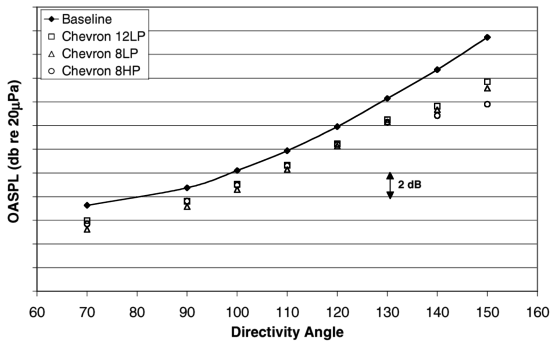

Fig. 8 Far-field OASPL directivity: nominal shear condition.

A. OASPL Mapping Results

The baseline mapping of OASPL for the nominal shear condition is shown in Fig. 13a. The peak noise generation region can be seen to extend from approximately 2–10 equivalent diameters downstream of the fan nozzle exit plane. It is also notable that there appear to be two separate, but distinct, regions of peak noise. The first peak region occurs between two and four equivalent diameters with the second peak region occurring between seven and 10 equivalent diameters. It is possible that the upstream of these two sources is generated by the fan stream shear layer, while the more downstream region is

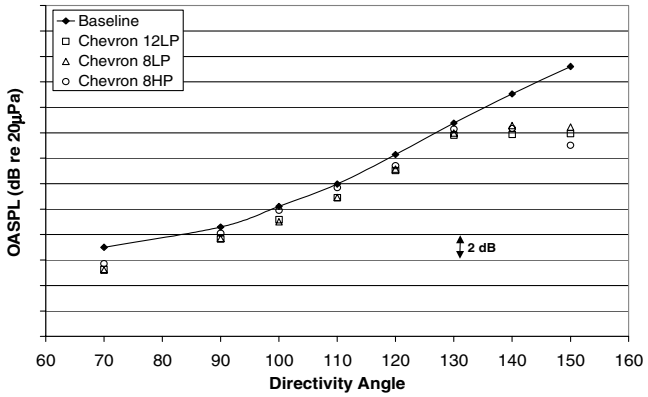

Fig. 9 Far-field OASPL directivity: high shear condition.

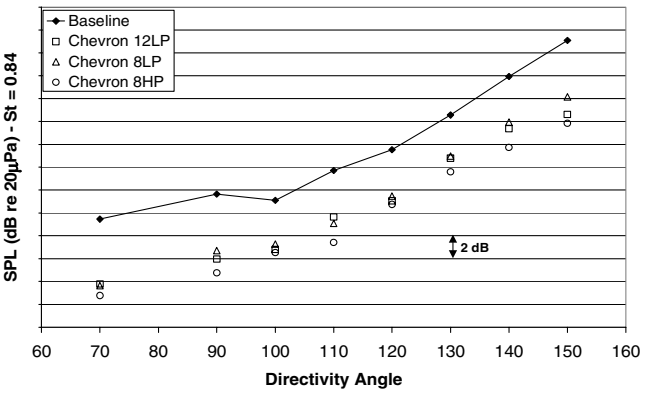

Fig. 11 Far-field low-frequency directivity ($St = 0.84$): high shear condition.

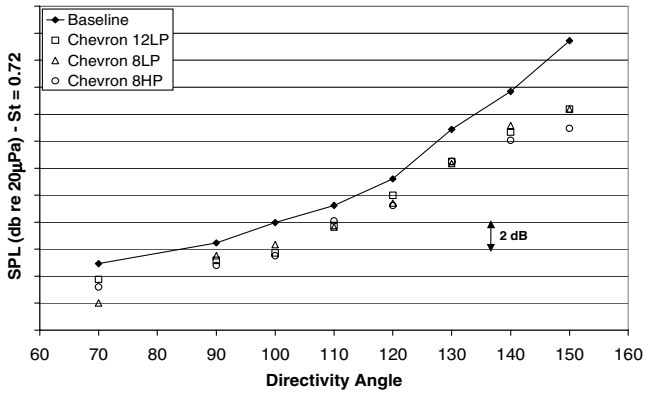

Fig. 10 Far-field low-frequency directivity ($St = 0.72$): nominal shear condition.

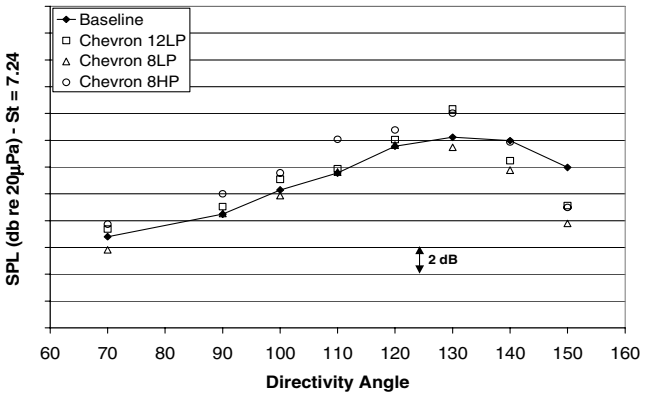

Fig. 12 Far-field high-frequency directivity ($St = 7.24$): nominal shear condition.

generated by the breakdown of the jet potential core. This latter hypothesis is supported by particle imaging velocimetry (PIV) data obtained by Bridges and Wernet [13], which indicates a potential core length of approximately 7–10 equivalent nozzle diameters for a jet operating under similar conditions. Although further circumstantial evidence will be presented throughout this work to support these suggestions, a rough comparison shows these suggested source regions to be consistent with near-field phased array data presented by Agboola and Bridges [14] for a similar jet geometry and operating condition. Specifically, Fig. 4 in this reference shows the peak jet noise frequencies to occur at axial distances in excess of five diameters. Higher frequencies, typically associated with smaller scale shear layer structures, are seen at distances of less than two diameters. It is also interesting to note that this downstream noise region seen in the near-field mapping extends beyond the end of the mapping grid, indicating the presence of significant noise sources at axial distances in excess of 10 equivalent diameters. This is consistent with the far-field OASPL directivity, which is shown in Fig. 8. In this figure, note that the far-field array does not capture the peak OASPL emission angle for the baseline case, which would also indicate the presence of additional downstream sources.

OASPL mappings at the nominal shear condition for the three chevron nozzles are presented in Figs. 13b–13d. Here, it is clear that the chevron nozzles modify the acoustic near field, most notably by reducing the size of the peak noise region. The peak noise region of the baseline nozzle has been reduced from two to 10 equivalent diameters to one to six diameters for each of the chevron nozzles, with noise reductions of 4–6 dB being observed downstream of seven diameters. It is also notable that there is no longer an observable separation of the peak noise into two distinct regions. The reduction in the noise downstream of six diameters indicates that the chevrons have primarily impacted the more downstream of the two noise generating regions. If this downstream noise is attributable to potential core breakdown, these results would be consistent with observations made by other researchers which show that mixing enhancement devices, such as chevrons, can shorten the jet potential core [1,3,11]. The upstream shift and reduction in size of the peak noise generation region is also consistent with the far-field OASPL directivity data shown in Fig. 8. Although the far-field peak emission angle was not captured for the baseline nozzle, it appears that the OASPL is beginning to peak by 150 deg for each of the chevron nozzles. This also indicates that the chevrons have acted to reduce the axial extent of the jet noise source distribution. Finally, it appears that the peak OASPL intensity is increased slightly by the chevrons just downstream of the core exit plane at an axial distance of three to four equivalent diameters. The exact cause of this increase will become clear later.

The relative effects of the three chevron nozzles on OASPL show very subtle differences. For example, the peak noise region in the range of two to five equivalent diameters extends slightly further in the radial direction for the high penetration nozzle than for either of the nominal penetration nozzles. This can be seen by comparing the shape of the contours at an axial position of four diameters and a radial position of approximately one diameter. Also, observation along the inner edge of the mapping grid indicates that the high penetration nozzle is slightly quieter downstream of approximately eight equivalent diameters. The reasons for these differences will become apparent in later sections. The subtle differences among the three chevrons seen in the OASPL near field are consistent with the far-field spectra shown in Fig. 8, which also indicates only minor differences in the three chevron nozzles.

Figure 14a shows the baseline OASPL mapping for the high shear operating condition. At this operating condition the peak noise region no longer shows the separation that it did for the nominal shear condition. Based on the fact that the peak noise region now occurs between four and 10 equivalent diameters, it appears that the more upstream noise generation region is contributing less significantly. In discussion of the nominal shear results, it was suggested that this

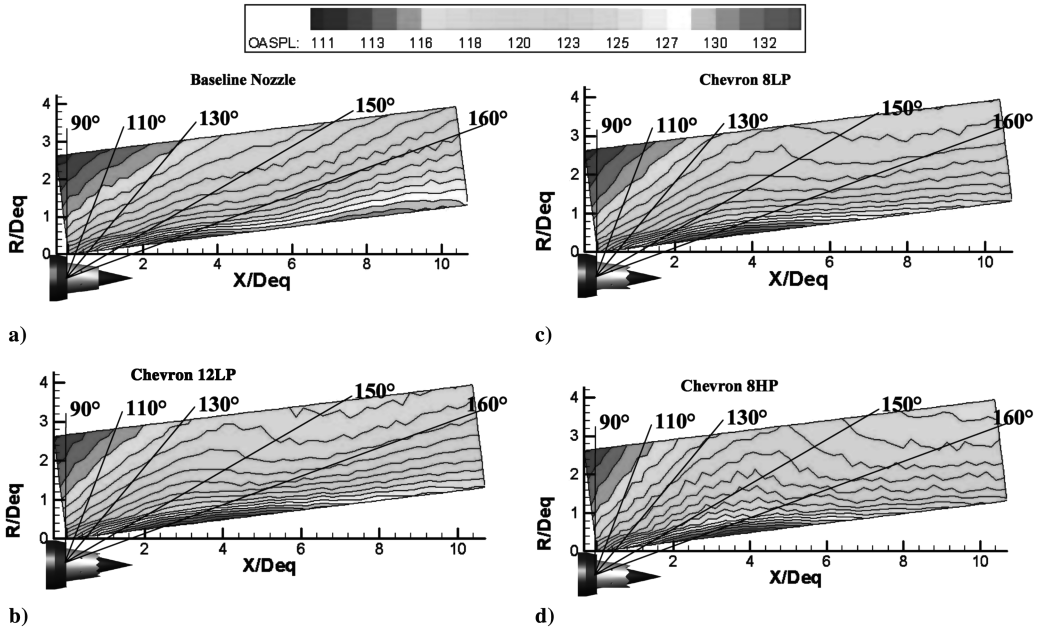

Fig. 13 a)–d) Nominal shear condition OASPL mappings.

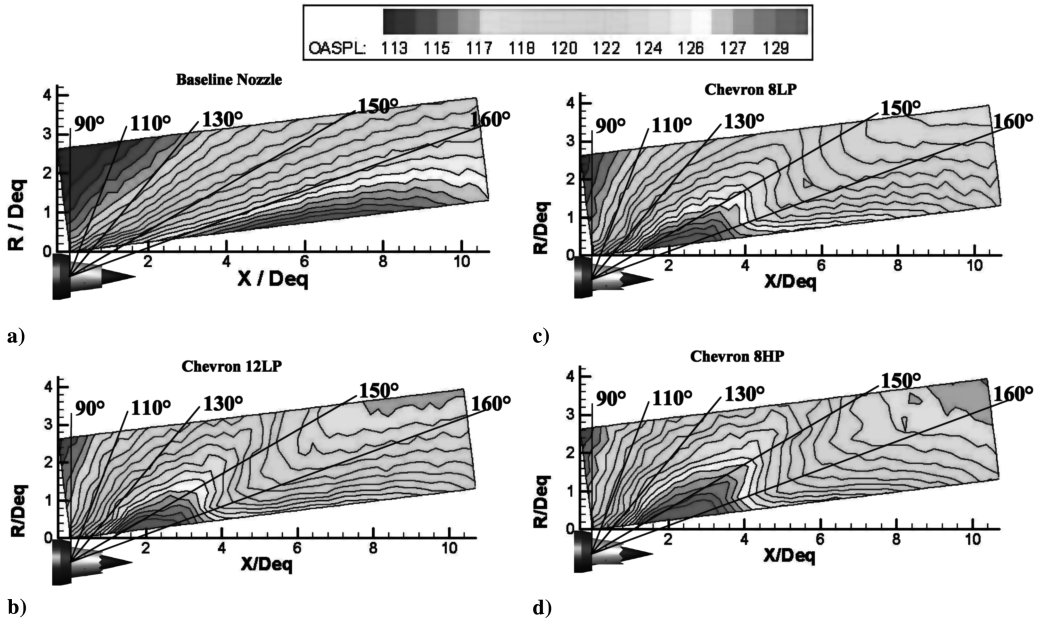

Fig. 14 a)–d) High shear condition OASPL mappings.

upstream region could be attributable to the fan stream shear layer. The high shear results would lend credibility to suggestion because the fan stream velocity has been reduced, relative to the nominal shear condition, and this region now shows lower noise levels. As a result of this, the downstream noise region appears to be the dominant noise generator at this operating condition. In Fig. 13a, it was argued that this downstream region was related to the breakdown of the jet potential core. Figure 14a supports this argument. It has been well documented that in a coflowing jet, the potential core length reduces as the shear velocity increases [15]. Therefore, as the fan velocity has been roughly halved from that of the nominal shear condition, it would be expected to see a reduced potential core length. If the downstream noise source noted in Fig. 13a is indeed related to the potential core breakdown, one would expect to see a corresponding upstream shift in the location of this noise source in Fig. 14a. This is exactly what is observed when comparing the mappings of Figs. 13a and 14a. The peak noise region, believed to be associated with the potential core breakdown, has shifted upstream from seven to 10 diameters to five to nine diameters.

For the high shear condition, the chevrons again produce substantial changes to the OASPL near field. Figures 14a–14d show comparisons of the OASPL mappings for this condition. The most dramatic noise reductions are again seen at downstream locations with reductions of nearly 10 dB being seen downstream of five diameters. In addition to these reductions being more dramatic than those observed at the nominal shear condition, the reduction in size of the peak noise region is also more significant. The peak generation region has been reduced from the five to nine equivalent diameters seen in the baseline case to one to four equivalent diameters. This implies that the mechanisms leading to these effects are stronger at this shear condition than at the nominal shear condition and supports the conclusion reached in the far-field study that the effectiveness of a given chevron design is directly related to the nozzle shear velocity. At this condition, the chevrons also appear to impact the OASPL

directivity pattern, as each of the three chevrons show very clear lobes propagating into the 130 to 150 deg sector. This shift in the OASPL directivity pattern is consistent with the far-field OASPL directivity seen in Fig. 9. In this figure, the chevrons shift the OASPL peak emission angle from somewhere in excess of 150 deg to approximately 130 to 140 deg. Although the OASPL mappings do not allow conclusions to be drawn in regard to the chevron effects on various frequencies, the significant noise reductions seen at axial locations beyond five diameters do allow some information to be inferred. The phased array results of Agboola and Bridges identify the peak low-frequency noise generation region of a similar jet to occur at axial distances between five and 10 diameters. It has been well documented in the works of Tam [16] that these low frequencies are generated by large-scale turbulence structures which radiate noise preferentially to higher inlet angles. By reducing this downstream region of peak region of noise, the chevrons have effectively made the smaller scale structures, which exist closer to the nozzle exit plane, the primary noise generators. Because it is well accepted that these smaller scale structures radiate to more lateral inlet angles, this explains the shift in peak noise directivity seen in the far-field results of Fig. 9.

The relative effects of the three chevron nozzles are consistent with the observations made in the nominal shear case. However, the differences between the chevrons appear to be more emphasized by the higher nozzle shear velocity. Specifically, the additional downstream attenuation provided by the higher penetration nozzle, 8HP, is more evident than it was at the nominal shear operating condition. Comparing this nozzle with the nominal penetration nozzle of the same chevron count, 8LP, shows an additional 3–4 dB reduction at axial distances in excess of six equivalent diameters, indicating that the high penetration nozzle has a greater impact on the downstream regions. Another consistency with the nominal shear condition results is seen at an axial distance of one to four diameters where the peak noise penetrates further in the radial direction for the high penetration nozzle than for either of the two nominal penetration nozzles. Differences in nozzle 12LP and 8LP are again almost imperceptible. Based on these observations, together with the far-field study, it is concluded that the chevron penetration has a greater influence on the acoustic field than does the number of lobes.

Although the OASPL mappings presented in this section allow observations to be made in regard to the gross changes to the acoustic near field, it is necessary to look at individual frequency bands to better understand the source effects of the chevrons. These mappings will be presented in the following sections.

B. Low-Frequency Mapping Results

For the nominal shear condition, the low frequency corresponds to a mixed velocity Strouhal number ($St = f \cdot D_{eq}/V_{mix}$) of 0.72. The low-frequency mappings for this operating condition are presented in Figs. 15a–15d. The baseline case shows a region of peak noise that extends along the entire axial distance of the mapping grid. Beyond a distance of seven diameters, this region spreads outward in the radial direction. As suggested in the previous section, and supported by other published research efforts, this downstream region of low-frequency noise is likely related to the breakdown of the jet potential core.

The effect of the chevron nozzles on the low-frequency noise is quite dramatic. The noise region downstream of five diameters is suppressed by 5–7 dB by each of the three chevron nozzles. The fact that the noise upstream of two diameters does not appear to be significantly affected by the core chevrons provides further evidence that this noise is generated by the fan stream shear layer. The changes to the near-field structure are consistent with the far-field directivity at the same mixed velocity Strouhal number, which is shown in Fig. 10. Although the chevrons do not appear to be producing a significant change in the peak far-field directivity of the low-frequency noise, the increased acoustic benefit at angles beyond 130 deg is clearly consistent with the near-field results.

At low frequency, there appears to be only subtle differences in the relative effects of the chevrons. Close comparison of the three nozzles along the inner edge of the mapping grid indicates that the higher penetration nozzle produces more noise reduction downstream of eight diameters. Other than this difference, it appears that each of the chevrons produces a very similar effect on the near field at this Strouhal number. This similarity implies that the lower frequencies could be less sensitive to the geometric parameters explored in this study, at least for this operating condition.

Low-frequency comparisons for the high shear condition are presented in Figs. 16a–16d. This condition corresponds to a mixed velocity Strouhal number of 0.84. The baseline nozzle again shows a very strong region of low-frequency noise propagating outward from the jet axis. This peak noise region completely dominates the near field at directivity angles beyond 160 deg. The most intense region of the noise seems to be centered between five and 10 diameters, which is roughly consistent with the most intense region of the baseline OASPL shown in Fig. 14a. Again, it is notable that this region does not show the peak noise upstream of two diameters that was seen in Fig. 15a for the nominal shear condition. Because the fan stream velocity has been reduced relative to the nominal shear condition,

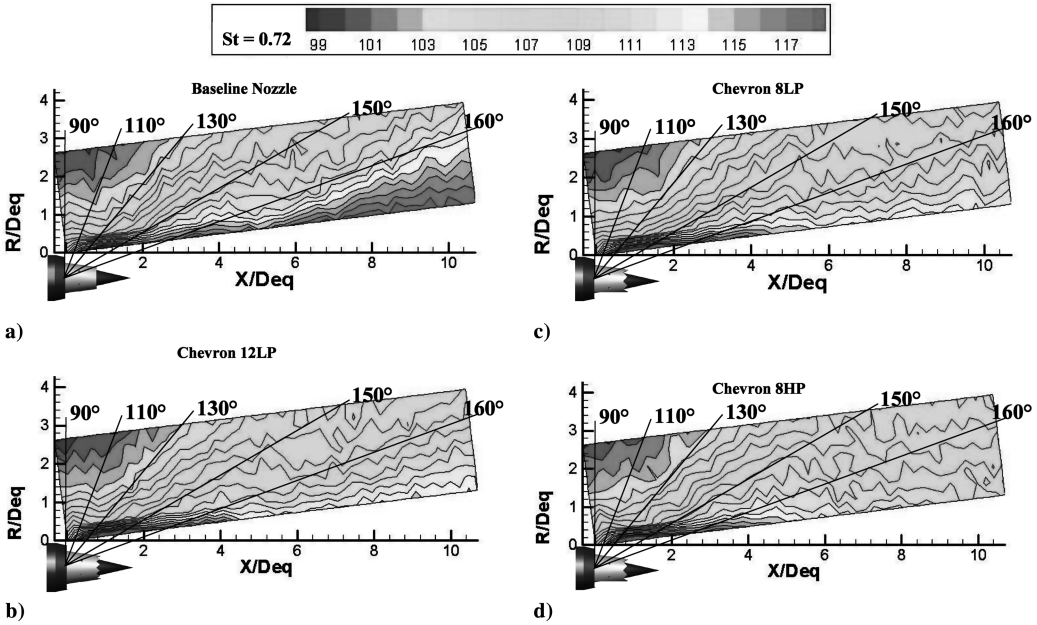

Fig. 15 a)–d) Nominal shear condition $St = f \cdot D_{eq}/V_{mix} = 0.72$ mappings.

this trend supports the suggestion that the fan shear layer is contributing to noise upstream of two equivalent diameters in the nominal shear case.

Outside of the noise upstream of two diameters, the chevron effects at this operating condition are fairly similar to those shown at the nominal shear condition. Again, the large noise region downstream of five diameters is suppressed by 5–7 dB. A small region of high noise remains at an axial location of two to five nozzle diameters for each of the three nozzles. As with the nominal shear case, it does not appear that the chevrons are producing a significant change in the directivity at this Strouhal number. This is also consistent with the far-field directivity results for the same operating condition. In Fig. 11, the far-field data show a fairly constant 4–6 dB reduction at all measured angles with little change in the directivity pattern.

Although the differences in the three chevrons remain relatively subtle at this operating condition, they are somewhat clearer than they were in the nominal shear case. The most significant differences are seen between the high penetration nozzle, 8HP, and the nominal penetration nozzles. The noise levels along the inner edge of the mapping grid show that this nozzle provides greater suppression at axial distances in excess of six diameters. Comparison of the two nominal penetration nozzles indicates that the eight lobe design is slightly noisier along the edge of the grid in an axial range of one to five diameters. However, on the whole, the differences in the three chevrons at this Strouhal number remain quite subtle. The implication of both the nominal and high shear condition results is that the acoustic near-field structure is relatively insensitive to the geometric parameters of penetration and number of lobes at low frequencies. However, the data suggest that there is greater sensitivity to the effects of penetration than the effects of the chevron count.

C. High-Frequency Mapping Results

The high-frequency mappings correspond to mixed velocity Strouhal numbers of 7.24 and 8.42 for the nominal and high shear conditions, respectively. The mappings for the nominal shear condition are presented in Figs. 17a–17d. The baseline sound field demonstrates a completely different behavior from the low-frequency mapping shown in Fig. 15a. The peak noise region has now separated into two distinct regions, which appear in similar axial locations to what was observed in the OASPL mapping of Fig. 13a. However, the two regions now appear much more distinctly. The more upstream region extends in the 130 deg direction and is centered at an axial location of approximately one diameter. This region generates the highest noise levels at approximately 108 dB. The downstream noise begins at an axial distance of six diameters, extends to approximately 10 diameters, and appears to propagate to angles between 150 and 160 deg. This source region shows lower peak levels than that of the more upstream region. Throughout this work, it has been hypothesized that the upstream source region is associated with the fan shear layer, whereas the more downstream source is associated with the breakdown of the jet potential core. The high shear condition results will provide yet further evidence to support this argument.

At this frequency and operating condition, the chevrons significantly alter both the near-field structure and the apparent directivity. The noise downstream of six diameters has been suppressed by 4–7 dB, whereas the noise upstream of four diameters has been increased by up to 7 dB. An interesting observation can be made in regard to the location and intensity of the increased noise region. Note that it does not correspond to the location of the noise that has been attributed to the fan nozzle shear layer, which is roughly centered at one diameter. Rather the peak noise of the chevrons appears to be centered at approximately two to three diameters. This corresponds to an axial location just downstream of the core nozzle exit plane. Because it is known that chevrons increase mixing, it is likely that this increased high- frequency noise is a byproduct of increased turbulence in the initial development region of the core nozzle shear layer. Further evidence to support this argument will be offered in the discussion of the high shear condition results. The overall effect of the downstream suppression and the upstream noise increase is to change the apparent directivity. The baseline mapping showed the upstream lobe to propagate principally toward the 130 deg angle, whereas the downstream source region propagated to higher angles. The downstream suppression of the chevrons has virtually eliminated any evidence of the higher angle propagation. At the same time, the upstream lobe has been strengthened. The net result is a single lobe of high-frequency noise that appears to propagate to the 120 to 140 deg sector. These results compare well with the far-field directivity of this frequency band, which is shown in Fig. 12. This shows the noise of the baseline nozzle to peak at approximately 140 deg. This likely is due to the combined effects of the upstream and downstream source regions seen in Fig. 17a. In contrast, each of the chevron nozzles shows a peak level occurring at approximately 130 deg. In addition, each of the chevrons show increased SPL relative to the baseline at angles upstream of this. These changes in far-field directivity are consistent with the changes in the near-field structure seen in Fig. 17.

At this frequency band and operating condition, the individual chevrons begin to show identifiable differences. These differences include the peak SPL as well as directivity effects. The most significant differences are seen between the higher penetration nozzle and the two nominal penetration nozzles. Although the nominal penetration nozzles show similar effects, the higher penetration nozzle clearly shows a much larger peak noise region, as well as higher noise levels. This result supports the suggestion that the peak noise region is related to increased turbulence in the core shear layer that is induced by the chevron mixing. It is clear that the higher penetration design would induce stronger vorticity, which would logically lead to higher turbulence levels. In addition, the higher penetration nozzle appears to also generate more noise at the forward angles. This can be seen by looking closely along the 90 deg angle at radial locations greater than two diameters. Figure 12 also shows chevron 8HP to be the noisiest at all forward angles. The differences between the two nominal penetration nozzles are more subtle. However, close observation reveals that the 12 lobe design has a slightly larger peak noise region than the eight lobe design. These observations are all consistent with the far-field investigation, which concluded that the chevron penetration was the primary geometric parameter influencing the acoustic benefit. The number of chevrons was determined to have a secondary effect. These results have provided additional insight into the high-frequency noise generation of chevrons. By determining that this noise propagates from the region just downstream of the core nozzle exit plane, these mappings provided solid evidence to link increased shear layer turbulence, due to chevron mixing, with this high-frequency noise generation.

Figures 18a–18d present the near-field mappings for the high shear operating condition at a mixed velocity Strouhal number of 8.42. The baseline nozzle shows a fairly uniform near field for the selected contour level, with the maximum levels extending from one to nine equivalent nozzle diameters. Although the sound field does not initially appear to demonstrate the same division that was seen at the nominal shear operating condition, close inspection does indicate the presence of two separate peak noise regions. The more upstream of these peaks remains at approximately one diameter, while the downstream peak is centered between five and six diameters. Again, it has been suggested throughout this work that the upstream source is associated with the fan nozzle shear layer. Further evidence to support this argument will now be presented. Consistent with the argument made in discussion of the OASPL results, the reduction in fan stream velocity can be correlated to a reduction in noise associated with the upstream region. Recall that at the nominal shear condition, the highest peak levels of approximately 108 dB corresponded to the more upstream source region, while the downstream region showed levels that were 3–4 dB lower. Based on the lower fan stream velocity, and the reduced fan shear layer gradient, it would be expected to see reduced noise levels associated with this noise region at the high shear operating condition. This is exactly what is shown by Fig. 18a, which shows that the peak levels of the upstream and downstream source regions are now roughly equal. Furthermore, Fig. 18a shows that the downstream source

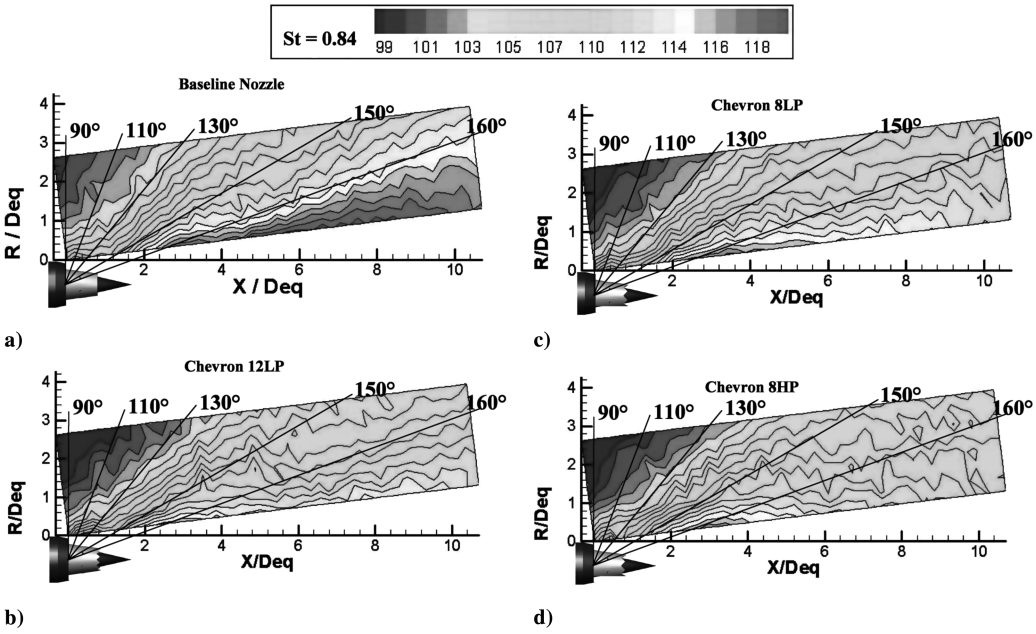

Fig. 16 a)–d) High shear condition $St = f \cdot D_{eq}/V_{mix} = 0.84$ mappings.

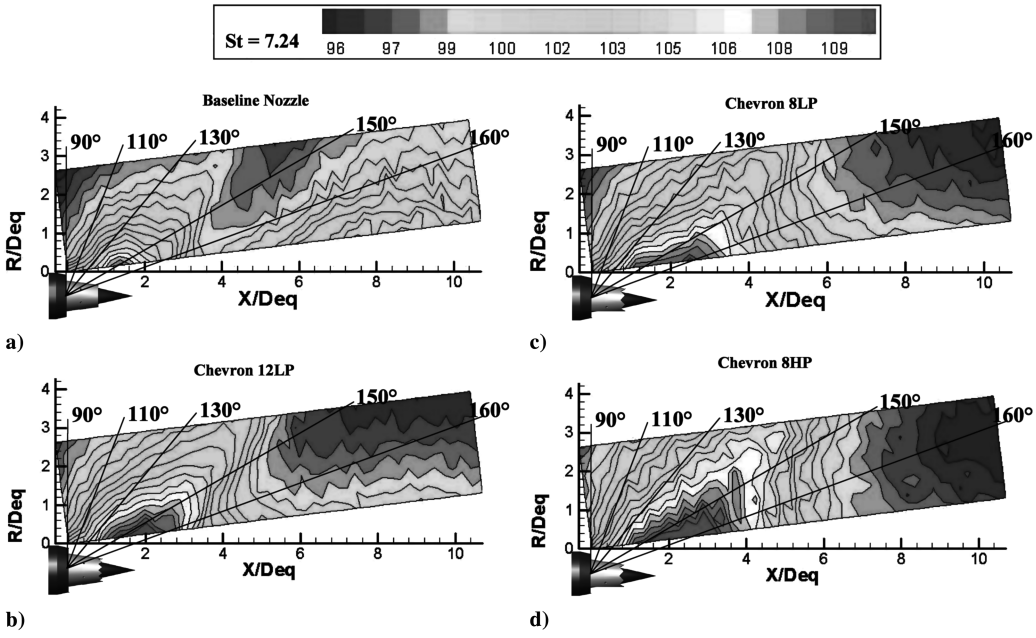

Fig. 17 a)–d) Nominal shear condition $St = f \cdot D_{eq}/V_{mix} = 7.24$ mappings.

region has moved upstream to approximately five diameters as opposed to the nine diameters that was shown for the nominal shear condition. Because of the increase shear gradients in the core nozzle shear layer, this provides further evidence to support the argument that this noise region is associated with the end of the jet potential core. The changes in magnitude and location of the two source regions correspond well with documented evidence of jet noise source changes with operating condition. This provides evidence to corroborate the suggestions made in previous sections regarding the generation mechanism responsible for the two noise source regions. The ability to confidently associate the noise generation regions with known jet noise behaviors is important to be able to draw conclusions in regard to the chevron effects.

Recall that this frequency corresponds to the point of maximum high-frequency SPL increase in the far-field spectra. A simple glance at the chevron mappings makes the source of this high-frequency crossover clear. While the chevrons are providing SPL reductions of 5–6 dB at some of the downstream locations, each can be seen to be generating significant high-frequency noise just downstream of the core exit plane. Local SPL increases in excess of 10 dB can be seen in this region. In discussion of the high-frequency results for the nominal shear condition, it was suggested that the increased noise region at two to three diameters is associated with increased mixing in the initial development region of the core shear layer. As the shear gradient between the core and fan streams is increased, it would be expected to see an accompanying increase in the shear layer turbulence. As a result, the effect of any mixing enhancement devices, such as chevrons, would be expected to be amplified. The increased noise generation seen at this condition, relative to the nominal shear condition, provides further evidence to support this argument.

At this operating condition, the differences between the three chevron designs are consistent with those seen at the nominal shear condition, yet more clear. Again, the largest differences are seen with

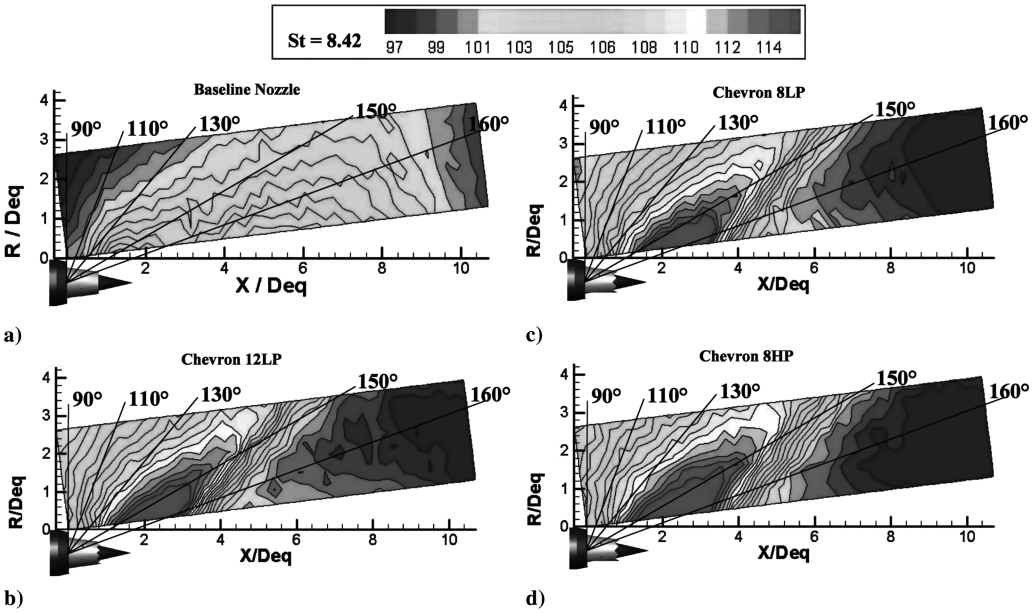

Fig. 18 a)–d) High shear condition $St = f \cdot D_{eq}/V_{mix} = 8.42$ mappings.

the change in penetration. The high penetration nozzle produces the largest noise increases and the spatial extent of this peak noise is clearly greater than that of either of the lower penetration nozzles. Comparison of the two nominal penetration nozzles shows that the 12 lobe design generates a peak noise region that is marginally larger than that of the eight lobe design. Again, these results are consistent with the far-field spectral results which identified chevron 8LP as the design which generated the least amount of high-frequency noise.

D. Relation of Near Field to Far Field

There is always a concern that measurements taken in the acoustic near field can be dominated by hydrodynamic pressures and decaying modes that do not propagate to the far field. Throughout this paper, attempts have been made to show consistency between the near-field and the far-field results. For the most part, these comparisons have shown good correlation, indicating that these near-field measurements are relevant to understanding the far-field effects.

It should also be stressed that the high-frequency noise increases seen for the chevrons do not necessarily lead to comparable increases in the far field. For example, the high-frequency mappings for the nominal shear condition show the chevrons producing increased noise near the nozzle exit plane. However, the far-field results for this condition do not indicate any noise increases in either spectral results (Fig. 7) or in OASPL directivity results (Fig. 8).

IV. Summary and Conclusions

The results of this study have provided insight into the mechanisms of core chevron nozzles that complements the previously completed far-field investigation. The previous study showed that the chevrons provided maximum acoustic benefit at aft angles and low frequencies. It was also shown that the nozzle operating condition played a large role in determining the acoustic benefit provided by a given chevron design. For example, the high shear condition was shown to produce high-frequency crossover in the aft angle spectra, while the nominal shear operating condition did not. Furthermore, the far-field investigation was able to identify differences in the relative effects of the three chevron nozzles. This led to the conclusion that the chevron penetration was a primary geometric parameter, which affected the acoustic benefit at all measured frequencies, while the number of chevron lobes was a secondary geometric parameter that primarily affected the higher frequencies.

The near-field mappings have provided further insight to the effect of the chevrons on noise generation and propagation. For both the nominal and high shear operation conditions, the near-field mappings identified two distinct peak noise regions. These were seen most clearly at the high frequencies. The core chevrons were shown to be most effective on the more downstream source region, with local SPL reductions as high as 7 dB being measured at axial locations downstream of approximately six equivalent nozzle diameters. In contrast to this, the near-field mappings also identified increased noise regions that were directly correlated to the high-frequency crossover effects seen in far-field results. The data showed significant increases in noise propagating from an axial distance of two to three diameters downstream of the fan nozzle exit plane. Increases as high as 7–10 dB were measured depending on the nozzle operating condition and the specific chevron design. Evidence was presented to indicate that this increased noise is associated with increased turbulence in the core stream shear layer due to the vorticity introduced by the chevrons. Finally, the near-field measurements supported the conclusions of the previously completed far-field study in regard to the critical chevron design parameters. Specifically, the nozzle shear velocity was shown to strongly influence the effect of a given chevron design on the acoustic near field and the chevron penetration was identified as the geometric parameter with the largest influence on the acoustic benefits. This study has provided new insights into the fundamental noise reduction mechanisms of core chevron nozzles.

References

[1] Bradbury, L. J. S., and Khadem, A. H., "The Distortion of a Jet by Tabs," *Journal of Fluid Mechanics*, Vol. 70, No. 4, 1975, pp. 801–813. doi:10.1017/S0022112075002352

[2] Ahuja, K. K., and Brown, W. H., "Shear Flow Control by Mechanical Tabs," AIAA Paper 89-0994, 1989.

[3] Samimy, M., Zaman, K. B. M. Q., and Reeder, M. F., "Effect of Tabs on the Flow and Noise Field of an Axisymmetric Jet," *AIAA Journal*, Vol. 31, No. 4, 1993, pp. 609–619.

[4] Ahuja, K. K., Manes, J. P., and Massey, K. C., "An Evaluation of Various Concepts of Reducing Supersonic Jet Noise," AIAA Paper 90-3982, 1990.

[5] Saiyed, N. H., and Bridges, J. E., "Tabs and Mixers for Reducing Low Bypass Ratio Jet Noise," AIAA Paper 99-1986, 1999.

[6] Saiyed, Naseem, H., Mikkelsen, Kevin, L., and Bridges, James, E., "Acoustics and Thrust of Separate-Flow Exhaust Nozzles with Mixing Devices for High-Bypass-Ratio Engines," AIAA Paper 2000-1961, 2000.

[7] Salikuddin, M., Martens, S., Janardan, B. A., Shin, H., and Majjigi, R. K., "Experimental Study for Multi-Lobed Mixer High Bypass Exhaust Systems for Subsonic Jet Noise Reduction—Part 2: Acoustic Results," AIAA Paper 99-1988, 1999.

[8] Gliebe, P. R., Brausch, J. F., Majjigi, R. K., and Lee, R., "Jet Noise Suppression," *Aeroacoustics of Flight Vehicles*, edited by H. H. Hubbard, Vol. 2, Acoustical Society of America, Hampton, VA, 1995, pp. 207–269.

[9] Callender, B., Gutmark, E., and Martens, S., "A Far-Field Acoustic Investigation of Chevron Nozzle Mechanisms and Trends," *AIAA Journal*, Vol. 43, No. 1, 2005, pp. 87–95.

[10] Callender, B., Gutmark, E., and DiMicco, R., "Design and Validation of a Coaxial Nozzle Acoustic Test Facility," AIAA Paper 2002-0369, 2002.

[11] Callender, B., "An Investigation of Innovative Technologies for Reduction of Jet Noise in Medium and High Bypass Ratio Turbofan Engines," Ph.D. Dissertation, Aerospace Engineering Department, Univ. of Cincinnati, Cincinnati, OH, 2004.

[12] Vishwanathan, K., "Aeroacoustics of Hot Jets," *Journal of Fluid Mechanics*, Vol. 516, Oct. 2004, pp. 39–82. doi:10.1017/S0022112004000151

[13] Bridges, J., and Wernet, M. P., "Turbulence Measurements of Separate Flow Nozzles with Mixing Enhancement Features," AIAA Paper 2002-2484, 2002.

[14] Agboola, F. A., and Bridges, J., "Jet Noise Source Localization Using Linear Phased Array," NASA TM-2004-213041, 2004.

[15] Petersen, R. A., and Sarohia, V., "The Effect of Forward Flight on the Noise and Flow Field of Inverted Profile Jets," *Journal of Sound and Vibration*, Vol. 93, No. 1, 1984, pp. 39–55. doi:10.1016/0022-460X(84)90350-X

[16] Tam, C. K. W., Golebiowski, M., and Seiner, J. M., "On the Two Components of Turbulent Mixing Noise from Supersonic Jets," AIAA Paper 96-1716, 1996.

W. Ng
Associate Editor